AGU ADVANCING EARTH AND SPACE SCIENCE

Water Resources Research

RESEARCH ARTICLE
10.1029/2021WR029860

An Experimental and Numerical Approach to Modeling Large Wood Displacement in Rivers

D. Panici[1,2]

[1]College of Life and Environmental Sciences, University of Exeter, Exeter, UK, [2]Faculty of Engineering and Physical Sciences, University of Southampton, Southampton, UK

Key Points:

- Transport of large wood (LW) at the river surface after an initial transient motion is observed in narrow areas of the channel
- Other theories on secondary cells prove inconclusive since only limited effects were observed at convergence points of flow velocity
- A novel approach and system of equations on acceleration induced by hydrodynamic forces is proposed and tested on experimental observations

Correspondence to:
D. Panici,
d.panici@exeter.ac.uk

Citation:
Panici, D. (2021). An experimental and numerical approach to modeling large wood displacement in rivers. *Water Resources Research*, *57*, e2021WR029860. https://doi.org/10.1029/2021WR029860

Received 22 FEB 2021
Accepted 1 JUL 2021

Abstract Large wood (LW) is used for river restoration, aquatic habitat conservation, and flood control; however, it can pose a threat to human life and the built environment. The formation of LW jams, river management strategies, and design of mitigation measures crucially all depend on how the large wood is transported along a river. This paper experimentally analyses at laboratory scale the motion of natural sticks in a long stretch of a straight channel (>16 m), when LW is released at different locations and with different flow conditions. Results show that instream large wood, following a transient motion shortly after being released at the water surface, tends to follow preferential patterns along the channel. Froude number and location of large wood input may provide an estimation of the LW location in downstream reaches. Several mechanisms of motion were observed, some of which were very common, including a frequent tendency to assume a tilted position with respect to the direction parallel to the flow. The experiments also suggest that theories on secondary cells responsible for channeling LW in preferential directions are incomplete. A new model, based on acceleration induced by hydrodynamic actions, has been established and proposed in this work, showing promising results and paving the way for the development of a comprehensive model for transport of large wood at the river surface in full-scale applications.

1. Introduction

Large wood (LW), large wood debris, woody debris, instream wood or simply debris, are the widely known names for instream large trees and branches - normally of length >1 m and average diameter >10 cm (e.g., Gippel et al., 1996; Ruiz-Villanueva et al., 2019) although other definitions are also found based on qualitative features (e.g., Bradley et al., 2005), or scaled with the size of the watercourse (e.g., Ruiz-Villanueva, Piégay, Gaertner, et al., 2016; Ruiz-Villanueva, Piégay, Gurnell, et al., 2016). Over the decades, interest in the management of LW and the effects of LW on riverine environments as well as on the built environment has substantially grown. On one hand, LW is believed to benefit aquatic environment by providing biodiversity to fish habitat and stabilizing micro-organisms (Abbe & Montgomery, 1996; Gregory et al., 1993; Lagasse et al., 2010). Engineered LW jams can also be used to mitigate flood peak flows and stabilize river channels in order to restore natural river processes (Gurnell et al., 2019), whilst LW is also an important factor for geomorphological changes of the river (Mao et al., 2020). On the other hand, uncontrolled transport of LW accumulating at riverine structures can cause increased flood levels and hydraulic actions that may result in serious hazards to human life and infrastructure (Comiti et al., 2016; Lassettre & Kondolf, 2012).

In recent years, a significant amount of research has been devoted to unravel the complex interactions between LW, flow and structures; for example, LW entrapped at single bridge piers can form very large accumulations (Gschnitzer et al., 2017; Panici & de Almeida, 2020a; Panici et al., 2020), depending on flow and LW characteristics (Gschnitzer et al., 2017; Panici & de Almeida, 2018, 2020b); furthermore, accumulated LW can dramatically exacerbate local scour to single piers (Ebrahimi et al., 2018, 2020; Pagliara & Carnacina, 2011, 2013) or to array of piers (Schalko et al., 2019a). Accumulations of LW at in-line structures can also increase the backwater profile depending on the size and packing capacity of the accumulation (Panici & Kripakaran, 2021; Schalko et al., 2018). In some cases mitigation measures can be employed, including bypasses (Schmocker & Weitbrecht, 2013), in-line full-width racks (Schalko et al., 2019b), in-line alternating racks (Panici & Kripakaran, 2021), fins and sills (Bradley et al., 2005; Lyn et al., 2003; Schalko et al., 2019b).

A crucial aspect of the aforementioned effects and measures is related to the transport of LW in rivers, since jam formation and entrapment may depend on the characteristics of LW motion in rivers. Some studies focused on the initiation or mobilization of LW elements lying on the floodplains and being mobilized during floods, mostly due to the combined effect of flotation and drag force (Braudrick et al., 1997; Crosato et al., 2013; Diehl, 1997; Lagasse et al., 2010; Ruiz-Villanueva, Piégay, Gaertner, et al., 2016; Ruiz-Villanueva, Piégay, Gurnell, et al., 2016). Other factors may also include LW element orientation at the motion onset (Braudrick et al., 1997; Crosato et al., 2013; Lagasse et al., 2010; Wilcox & Wohl, 2006), and LW length and diameter (Braudrick et al., 1997; Crosato et al., 2013; Curran, 2010; Ruiz-Villanueva, Piégay, Gaertner, et al., 2016; Ruiz-Villanueva, Piégay, Gurnell, et al., 2016). LW elements can be recruited at different locations across a river channel depending on the main recruitment process; for example, bank erosion (Diehl, 1997; Lyn et al., 2003), banks mass-wasting and mass movement, dead plant, logging, windthrow, collapse from ice and snow (Diehl, 1997; Gurnell et al., 2019; Hassan et al., 2016; Lagasse et al., 2010; Pfister et al., 2013; Sedell et al., 1988) are the most common causes. The input of LW can therefore occur virtually at any point on a river section. Once LW elements are mobilized, they normally float at the river surface, provided that the wood density is lower than the water density and in consideration that wood density may have a significant effect on wood buoyancy and mobility (Ruiz-Villanueva, Piégay, Gaertner, et al., 2016; Ruiz-Villanueva, Piégay, Gurnell, et al., 2016). Previous flume experiments (Braudrick et al., 1997) were employed to identify three different modes of wood transport: *uncongested* (i.e., LW elements conveyed as single elements and with little or no interactions with other elements), *congested* (i.e., LW moving *en masse*) and *semi-congested*, that is, an intermediate condition. Field studies revealed that the uncongested mode of transport is the most frequently observed (Bradley et al., 2005; Diehl, 1997; Lagasse et al., 2010; Lyn et al., 2007), although hyper-congested flows (i.e., where the LW phase is highly concentrated and can overcome the liquid phase) have also been identified in extreme events and typically in mountainous areas (Ruiz-Villanueva et al., 2019).

Field observations revealed that, in the majority of the situations, LW is observed within a small portion of the channel (Bradley et al., 2005; Diehl, 1997), that often coincides with the point on the water surface where the depth is highest (Diehl, 1997; Lyn et al., 2003). In addition, transport of LW elements in these channel paths may recur when comparable flow conditions arise (Lyn et al., 2007). Nevertheless, reasons for this well-marked pattern are still unknown. Bradley et al. (2005); Diehl (1997); Lagasse et al. (2010) postulated that the path of LW on the water surface is driven by secondary currents (i.e., the flow velocity cells formed by velocity components normal to the streamwise direction) to the points of convergence on the water surface. This would explain why LW elements are normally observed in the centerline (for straight channels) and at the outer banks (for curved channels). However, this theory was not tested in the field nor corroborated with data, and thus could not be effectively proved (Lagasse et al., 2010). Past experiments seemed to confirm preferential patterns for both straight channel (Bocchiola et al., 2008) and curved reach (Schmocker & Weitbrecht, 2013), but could not provide any evidence to confirm the theory by Diehl (1997). De Cicco et al. (2020) observed in a flume experiment that LW elements released at the flume centerline occupied a narrow area of the flume center for $Fr = 0.50$, whilst for lower Fr (i.e., 0.30) the area was wider in either direction. Modeling of LW transport has been developed in the past, for which particular emphasis was put on incipient motion and LW-structure interactions, including CFD simulations (Mazzorana et al., 2011), and 2D hydrodynamic models (Ruiz-Villanueva, Piégay, Gaertner, et al., 2016; Ruiz-Villanueva, Piégay, Gurnell, et al., 2016), whilst comparatively less attention has been put on understanding the LW transport phenomena and its preferential patterns, or the influence of hydrodynamic actions.

A correct estimation of LW motion on the river surface can substantially increase the ability to assess risks at structures and design mitigation measures (Panici et al., 2020; Schalko et al., 2019a), plan and manage rivers for flood protection and habitat restoration, as well as improving our understanding of the fundamental physical phenomena that occur for these processes. The overarching aim of this work is to provide an understanding of the interactions between flow and LW for transport at the water surface. A series of laboratory experiments in a straight trapezoidal channel has been carried out in order to (a) analyze the patterns traveled by LW elements released at different locations along the channel, and (b) characterize the interactions between flow components and LW trajectories throughout the length of the flume by statistical analysis and physical modeling. The results from this work will pave the way for the development of accurate assessment of LW-related effects, together with effective planning for LW management.

2. Methodology

A dimensional analysis has been carried out to identify quantities relevant to the phenomenon of LW transport and also to provide similarity between experimental model and prototype. Dimensional analysis can also mitigate any scaling effect through dynamic similarity, whereby identical values of the resulting dimensionless quantities (including forces) at model and prototype scale are observed. An initial relationship among variables was defined as:

$$f\left(v,h,\rho,\mu,g,B,L,d,\rho_{LW},\delta\right)=0 \tag{1}$$

where v is the flow velocity, h is the flow depth, ρ is the flow density, μ is the flow dynamic viscosity, g is the gravitational acceleration, B is the top channel width, L is the LW length, d is the LW diameter, ρ_{LW} is the LW density, δ is the LW displacement. Applying Buckingham's Π theorem and choosing v, ρ, and h as repeated group, Equation 1 becomes:

$$f\left(\frac{\mu}{\rho vB},\frac{gB}{v^2},\frac{h}{B},\frac{L}{B},\frac{d}{B},\frac{\rho_{LW}}{\rho},\frac{\delta}{B}\right)=0 \tag{2}$$

where the first and second terms represent a form of Reynolds and Froude numbers, respectively. A few simplifications to Equation 2 can be done.

- The influence of LW density is tested as a constant value and its dimensionless ratio can be dropped from Equation 2.
- The length ratios L / B and d / B will be chosen sufficiently small to avoid frequent interactions with the channel walls; also, these ratios are kept constant for all experiments.
- The third dimensionless group (i.e., h / B) can be multiplied to the first two dimensionless groups, as it will be better descriptive of the observed hydraulics (i.e., corresponding Reynolds and Froude numbers).
- Reynolds invariance is assumed, since tests were conducted in turbulent regime and scaling effects due to viscous forces can be neglected; hence, the corresponding Reynolds dimensionless group is relaxed from Equation 2.
- Froude similarity between model and prototype will ensure dynamic similarity, eliminating scale effects from gravity and inertia.

The resulting dimensionless relationship is:

$$f\left(Fr,\frac{\delta}{B}\right)=0 \tag{3}$$

Equation 3 relates the displacement of LW elements to the flow characteristics. Thus, experimental tests and data analysis were designed to investigate the importance of the dimensionless variables in Equation 3 for LW motion. A series of three experimental campaigns has been carried out at the fixed trapezoidal recirculating flume at the University of Southampton Science Park. The prismatic flume is 54 m long and 3.25 m wide (at the major base) and 2.05 m wide at the minor base, that is, the flume bed. The flume height is 0.55 m. The angle at the flume sides corresponds to 42.5°. This type of flume was chosen for the following reasons:

- Wide channel width to maximize potential trajectories of LW elements;
- Higher variability of flow velocity (and, hence, of secondary cells and convergence points) due to the trapezoidal shape;
- Long stretch of the flume to allow tracking of elements;
- Moderate model-prototype scale (e.g., 1:5 to 1:20 for many lowland European rivers) to minimize potential scaling effects.

The flume is equipped with a sharp crested weir at the outlet for water level control. The inlet is also controlled by a drowned broad crested weir to allow pumping of the water contained inside the sumps. The flume is equipped with three pumps which combined together can reach a maximum discharge of 0.31 m^3s^{-1}. The flume could be accessed from any side and can be crossed through a fixed bridge at the inlet and

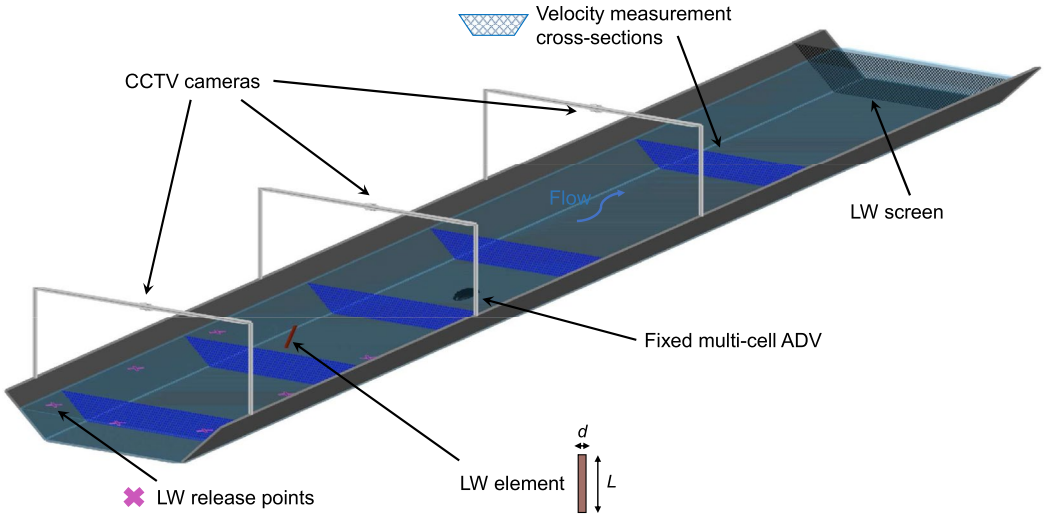

(a)

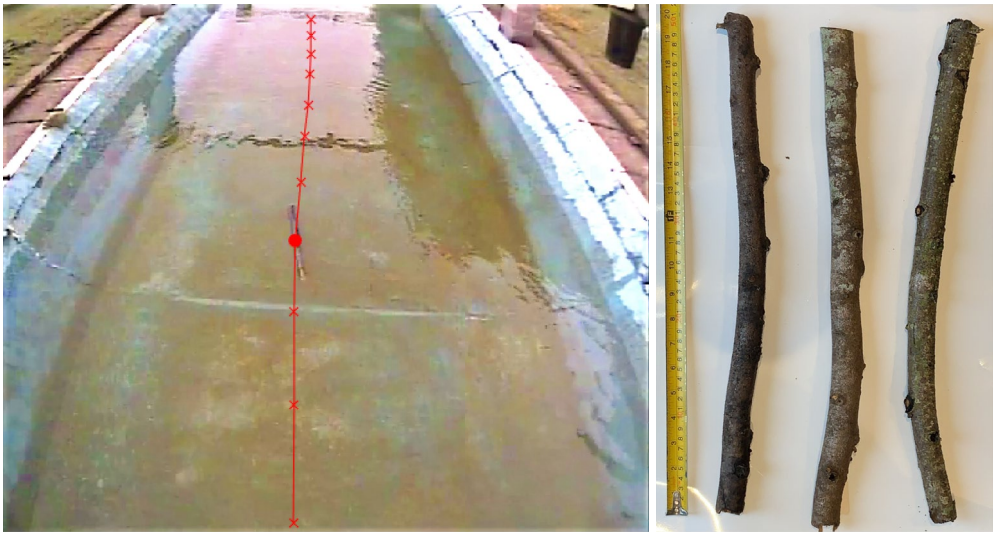

(b) (c)

Figure 1. (a) Sketch of the flume set-up indicating the experimental apparatus, measuring locations, acoustic Doppler-velocimeter (ADV), and a large wood (LW) element, (b) Frame from first CCTV camera (test group BC) that includes a tracking of a LW element in the distorted scale, (c) examples of LW elements used for the experiments.

a mobile gantry. The flume has a fixed gradient of 6×10^{-4}, and uniform flow conditions were achieved in the stretch where tracking was carried out.

The experimental set-up is sketched in Figure 1, where the 0 x-coordinate (i.e., the main flow direction) has been set 3 m downstream of the inlet to account for development of turbulence, whilst the y coordinate is set to 0 at the flume centerline and the z coordinate at the flume fixed bed. A series of three video-cameras in a CCTV system (sampling at 25 frames per second) was installed 1.2 m above the flume at distances $x = 2$ m, 7.5 and 13 m, respectively. Overall, the cameras covered a length of approximately 16 m. A reference grid was captured by the cameras prior to any experiment in order to map the undistorted x (i.e., parallel to the main flow direction) and y (i.e., perpendicular to the main flow direction) coordinates. The 3-D components of the flow velocity were measured by a SonTek Flow Tracker ADV (nominal accuracy ±1% of measured values) at five cross-sections, respectively at $x = 1$ m, 4 m, 7 m, 10 m, and 15 m. Such sections were chosen to provide spot measurements of flow velocity and compare if local velocity changes had influence

Table 1
Experimental Groups With Description of Flow and Location Characteristics

Group[a]	Water depth h (m)	Velocity v (m/s)	Froude number Fr	Dropping location
AL	0.208	0.165	0.121	Left
AC	0.208	0.165	0.121	Centerline
AR	0.208	0.165	0.121	Right
BL	0.261	0.250	0.165	Left
BC	0.261	0.250	0.165	Centerline
BR	0.261	0.250	0.165	Right
CL	0.257	0.418	0.279	Left
CC	0.257	0.418	0.279	Centerline
CR	0.257	0.418	0.279	Right

[a]First letter: A, B, C are Froude values in ascending order; Second letter: L, C, R are left, center, right release locations.

on the LW motion. Measurements at the cross-sections consisted of 36 points of measurements (sampling frequency 10 Hz), each averaged over 120 s. Discharge was constantly monitored by a SonTek IQ Plus multi-cell multi-beam ADV installed at the centerline of the flume bed at $x = 10$ m and was used to estimate the flow discharge together with the sharp crested weir equation for additional accuracy. The water level was measured at the beginning of each experimental campaign along the flume by using a point gauge (accuracy ± 0.25 mm). Flow conditions were established by controlling the downstream level using the weir height and also adjusting the discharge that was monitored by the IQ Plus.

Table 1 summarizes the experimental groups tested for this work, indicating flow properties and LW release location. Three different flow conditions were tested in the flume, for Froude numbers (where the characteristic length is the hydraulic mean depth $h_m = A / T$, for which A is the flow area and T is the top water surface width) of values 0.121, 0.165, and 0.279 (experimental macro-groups A, B, and C, respectively), which is typical for flood flows in lowland rivers. On the other hand, Reynolds number varied between 2.70×10^4 and 8.56×10^4. The underlying principle of the experiments conducted in this work has been to assume Reynolds invariance by disregarding Reynolds similarity and only consider Froude similarity between model and prototype, as it is a consolidated practice in hydraulic research (e.g., Bocchiola et al., 2008; Panici & de Almeida, 2018; Panici & Kripakaran, 2021; Wallerstein et al., 1997). In addition, since Reynolds number was kept $>10^4$ and water depth >0.05 m, potential scaling effects from viscosity and surface tension were minimized (Heller, 2011; Schalko et al., 2019b). Water levels varied between 0.205 and 0.261 m, whilst the cross-section averaged velocity varied between 0.165 and 0.418 ms^{-1}.

LW pieces were modeled by 48 defoliated natural sticks of length 0.50 m and average diameter 0.029 m standard deviation 0.003 m. Sticks from trees and branches have been preferred to idealized elements (e.g., dowels) since LW is best modeled using natural elements (Lyn et al., 2003; Panici & de Almeida, 2020b), and also for comparison with the growing literature on LW that makes use of these elements (e.g., Schmocker & Hager, 2011; Schalko et al., 2019b). The sticks were collected within the premises of the laboratory and are representative of British and European trees (e.g., beech and birch) and were selected as straight and regular as possible; the sticks underwent a cycle of soaking and drying until the average density of this material was approximately 550 kgm^{-3}. The sticks were individually released onto the water surface and at a rate < 1 in 5 s, in order to simulate an uncongested mode of transport and avoid interactions between elements; release was carried out manually and oriented parallel to the flow whenever possible (although in some cases slight initial angles could not be avoided) in accordance with field observations (e.g., Diehl, 1997; Sedell et al., 1988) that identified this orientation as the most frequently observed in rivers, and left free to be conveyed by the flow. The sticks were released at the cross-section $x = 0$ m, whereas three dropping points were located at the left bank, right bank and centerline respectively. For added stochasticity, some sticks at the right and left bank were released at the cross-sections $x = 3$ and 4.5 m. Each experimental group consisted of 16 sticks. The number of sticks per experiment (48) and experimental group (16) was chosen to provide sufficient variability to the types of LW transport, and was also similar to previous works on LW in flume experiments (e.g., De Cicco et al., 2020; Furlan et al., 2018; Schalko et al., 2019a; Schmocker & Hager, 2011). A porous screen was placed at the far end of the flume to prevent LW elements to reach the sumps; the screen was cleared regularly from accumulated elements to prevent affecting the upstream flow.

A total number of 144 tests was run for this work. Once each experiment was concluded, video-recordings were analyzed at a rate of 0.25 frames per second (fps), that is, 1 frame every 4 s (experiments AL, AC, AR); 0.5 fps, that is, 1 frame every 2 s (experiments BL, BC, BR) and 1 fps (experiments CL, CC, CR). Each captured frame was used to track the position of the center of mass (defined as the coordinates of the mid-point between the coordinates of the two ends of each element) of the LW elements along the whole length of the experimental area (16 m). Then, distorted coordinates were converted to the undistorted system by a custom algorithm based on a bilinear approach built on the reference grid recorded before the experiments. The

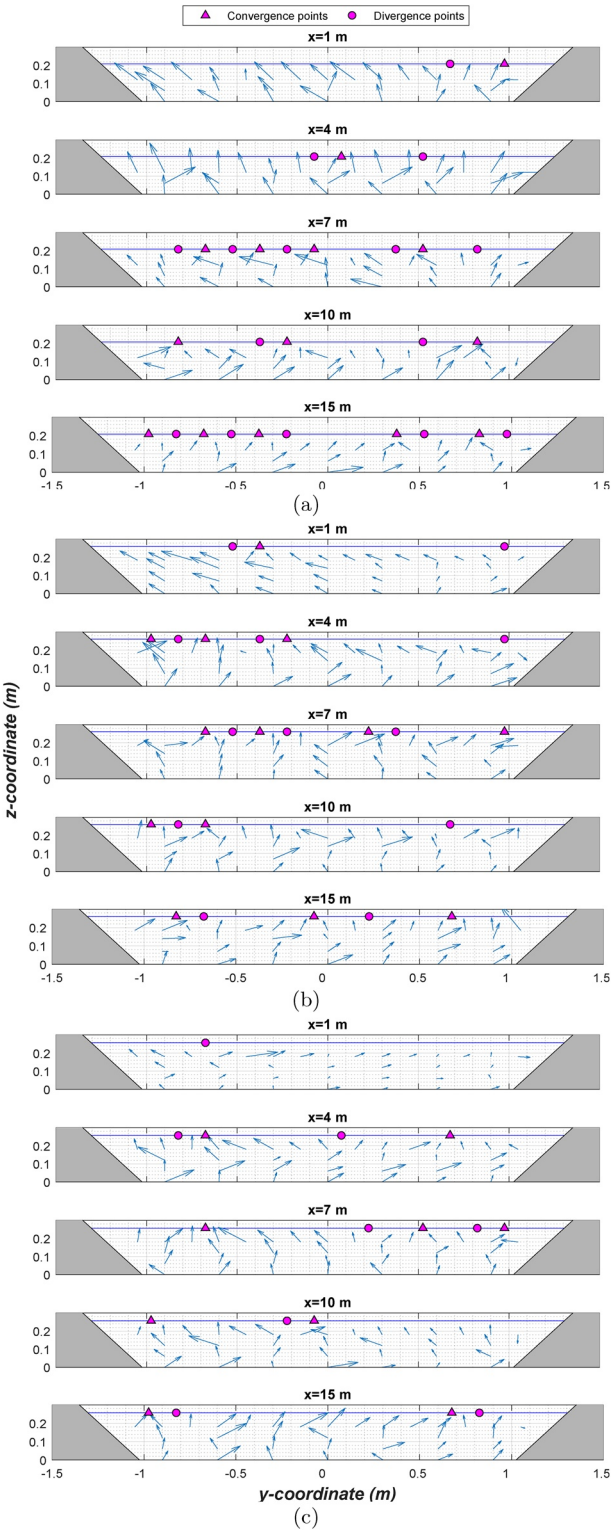

Figure 2. Velocity field for $Fr = 0.121$ (2a), 0.165 (2b) and 0.279 (2c) at the measured cross-sections. The blue lines indicate the water surface, whilst triangles and circles, respectively, the divergence and convergence points at the surface.

size of natural sticks used to model LW and flume width and length also improved visibility of elements in video recordings and minimized loss of accuracy due to capturing distorted scale. Figure 1 shows an example of a frame used for tracking from one of the CCTV camera system for a LW element in group BC with superposition of the tracking trajectory.

3. Results

In this section, the experimental observations are reported and described for all experimental groups, including measurements of the flow velocity, the trajectories of LW elements and the observed main mechanisms of motion.

3.1. Velocity Measurements

The velocity vectors at the five cross-sections along the flume are shown in Figure 2 for $Fr = 0.121$, 0.165 and 0.279 (top to bottom). The vectors are represented by arrows and are the sum of the y (i.e., horizontal) and z (i.e., vertical) components of the velocity, with respect to the flume walls and the water surface. The range of velocities observed at the water surface can vary widely, for example, for $Fr = 0.121$ velocity in the x-direction in all measured cross-sections is in the range 0.1434–0.2159 ms^{-1}, -0.0390 - 0.0331 ms^{-1} for y and −0.0077 - 0.0216 ms^{-1} for z. For $Fr = 0.165$, velocity in x ranges 0.1601–0.3254 ms^{-1}, in the y direction −0.0636 - 0.0394 ms^{-1} and in the z direction −0.0085–0.0333. Finally, for $Fr = 0.279$ it was measured for the x direction 0.2854–0.6367 ms^{-1}, for y −0.0843 - 0.0812 ms^{-1} and for z −0.0233 - 0.0458 ms^{-1}. Although varying significantly along the channel and cross-sections, the average values for x, y and z reflect approximately the cross-section averaged values measured by the multi-cell ADV. It is also notable to observe that, as expected, the x-component of water velocity can be up to 8 times greater than the y and z components.

At the water surface in Figure 2, points where two opposite y-components of the flow velocity are directed toward each other have been defined for the purpose of this study as *convergence* points, that is, points where secondary currents converge at the water surface. Similarly, points on the water surface where two opposite y-components of the flow velocity are directed away from each other, have been called in this study as *divergence* points, that is, a point on the water surface where secondary currents diverge.

At first, convergence and divergence points were observed at the water surface in all cross-sections and for all Fr conditions. In a large number of cases, two opposite points are located in adjacent positions (e.g., a convergence points next to a divergence point) indicating small-sized secondary cells. However, some marked differences can be observed. The amount of convergence and divergence points tended to decrease with the increase of Fr. For example, in section $x = 15$ m, five convergence points and five divergence points are observed for $Fr = 0.121$, three and two for $Fr = 0.165$, and two each for $Fr = 0.279$. A similar tendency can be observed for all other cross-sections. Furthermore, for lower Fr values a frequent alternation between convergence and divergence points is observed, often for adjacent points, meaning that for those conditions there

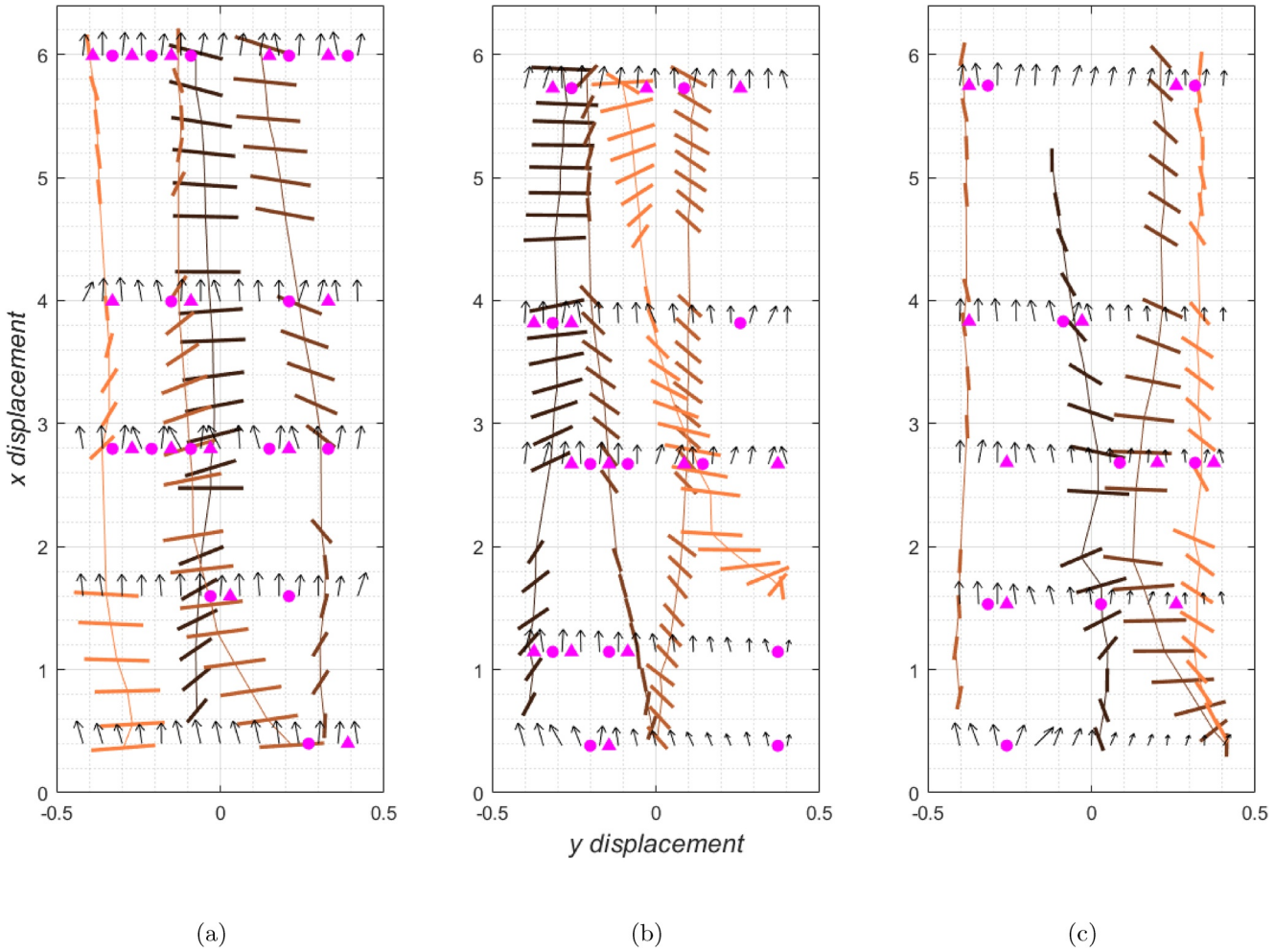

Figure 3. Tracked LW elements representing rotations and translations for $Fr = 0.121$ (3a), $Fr = 0.165$ (3b) and $Fr = 0.279$ (3c) including at least one element per experimental group in the dimensionless directions x and y (not represented in the same scale). Elements are represented by bars and solid lines represent the trajectory of the LW centers of mass. Figures also include velocity vectors (black arrows) and flow velocity convergence and divergence points (triangles and circles respectively).

is a high number of small cells. On the other hand, increasing Fr showed to provide a minor number of cells, but in wider sizes that may encompass large portions of the channel.

3.2. Tracking Large Wood Transport

The system of three cameras above the flume was employed to track the location of LW along the channel (Figure 1).

A first analysis can be undertaken for the observed rotational and translational motion of LW elements at the water surface for all Fr tested. Figure 3 shows some representative examples of the observed translational and rotational movements observed for LW elements at the flume surface for the three cases $Fr = 0.121$, 0.165, and 0.279 (sub-plots left to right). The x and y coordinates are made dimensionless via dividing the measured coordinate by the water surface width (constant in each experiment and of values, respectively, of 2.504 m, 2.620 and 2.611 m). Each sub-figure shows the motion of four different elements, in order to summarize the observations made for the most frequent types of motions and that are representative of the whole population of LW tested. The majority of elements (61.8%) were released at the surface with no apparent rotation relative to the main flow direction, whilst the remaining 38.2% of elements were released with a slight angle. Of the first group, only a small percentage of LW (10.1% of the initially straight elements,

that is 6.3% of the total number) effectively traveled along the flume keeping this orientation approximately unvaried. The remaining 89.9% of initially straight elements (or 55.6% of the total number of elements) were then either tilted with respect to the original position (of these, 31.2% clockwise and 43.8% anticlockwise, corresponding respectively to 17.4% and 24.3% of the total number of elements released) or ended up in a horizontal alignment, that is, perpendicular to the main direction of the flow (25% of initially straight elements or 13.9% of all elements). It is also important to note that the elements that retained a straight orientation were only those released at the two banks, whilst none were observed at the centerline. On the other hand, more than a third of tilted elements (i.e., 33.8%, or 15.3% of the total number of sticks) either from the initial position or during the experiments, reversed to a straight position. Elements that rotated until perpendicular to the flow typically (in 56.4% of the cases) reverted to a tilted position further on in the experiments, although none was observed to obtain a completely straight orientation. Other less frequent observations include: Elements with an already tilted direction increase their tilting angle only partially or changing direction of tilted angle (e.g., from a clockwise to an anticlockwise direction); elements that completely revolved about their center of mass for one or more times. The three different Fr conditions displayed the same types of rotation or translation consistently throughout the experimental campaign, with minimal differences that can be attributed to the stochasticity of the phenomenon.

Figure 4 shows the planar trajectories (lines) and coordinates of the tracked centers of mass (crosses) at the water surface of LW elements in the y (i.e., perpendicular to the flow) and x (i.e., parallel to the flow) directions for, respectively $Fr = 0.121$, 0.165, and 0.279. Similarly to Figure 3, the x and y coordinates are made dimensionless. Small gaps between $2< x <2.5$ and $4< x <4.5$ indicate areas where image definition was insufficient to obtain an accurate position, and therefore have been left blank. Blue crosses are the LW released at the left bank (groups AL, BL and CL), green crosses LW at the centerline (groups AC, BC and CC) and red crosses LW released at the right bank (groups AR, BR and CR). The x and y component of the measured water velocity at the water surface are included, together with convergence and divergence points as previously defined in Section 3.1.

Another observation about the LW trajectories concerns the ability of elements to spread out across the water surface for any tested Fr. Generally, the majority of elements tended to remain within the portion of the channel where they were originally released. Elements of groups AL, BL and CL were almost always observed for the coordinates $y < 0$ (except for a single point each for groups AL and CL and two elements of BL). Similarly, groups AR, BR, and CR remained mostly in the range $y > 0$, although in this case a total of eight (out of 48) elements crossed $y < 0$ and two (one each for AR and BR) even reached the area near the opposite bank. A similar (although slightly different) observation can be done for elements released at the centerline (i.e., AC, BC and CC). The majority of elements remained within the coordinates $-0.25< y < 0.25$, that is, half-width of the channel centered at the centerline, but a larger number of elements than other groups spread outside of this range, in several cases also reaching the areas near the flume banks. In general, spreading of elements trajectories is more evident for cases with low Fr, whereas for the highest Fr tested elements showed a tendency to remain in the channel area where originally released. This tendency occurred for the whole length of the flume, except for the initial stages of release: It is consistently observed in Figure 4, that y displacement is well-marked along the x direction for a dimensionless length of approximately 1, following release. This means that elements tend to spread out along the y-direction only for a distance of one channel width along the x-direction after being introduced on the water surface. Nevertheless, this tendency quickly disappears afterward and LW elements substantially reduce the rate of change in the y direction. This temporary phenomenon has been hereafter defined as *transient* motion. Another observation regards the different release locations on the left and right banks for groups AL, AR, BL, BR, CL, and CR. The trajectories resulting from these different locations showed a consistent trend with all the other release points; that is, limited spreading after the first transient motion and location well within the narrow part of the channel outlined in the above paragraphs.

The observations on LW trajectories are then compared to the velocity measurements along the water surface. While the x-component of the flow velocity has an observable importance in the trajectory of the LW elements, the same is not so immediately apparent for the y-component; for example, for $Fr = 0.121$ in Figure 4 elements of group AL at $x = 0.399$ are displaced opposite to the flow velocity on the y direction, whilst for group AC and AR large wood directions were oriented almost evenly in either direction, with unclear

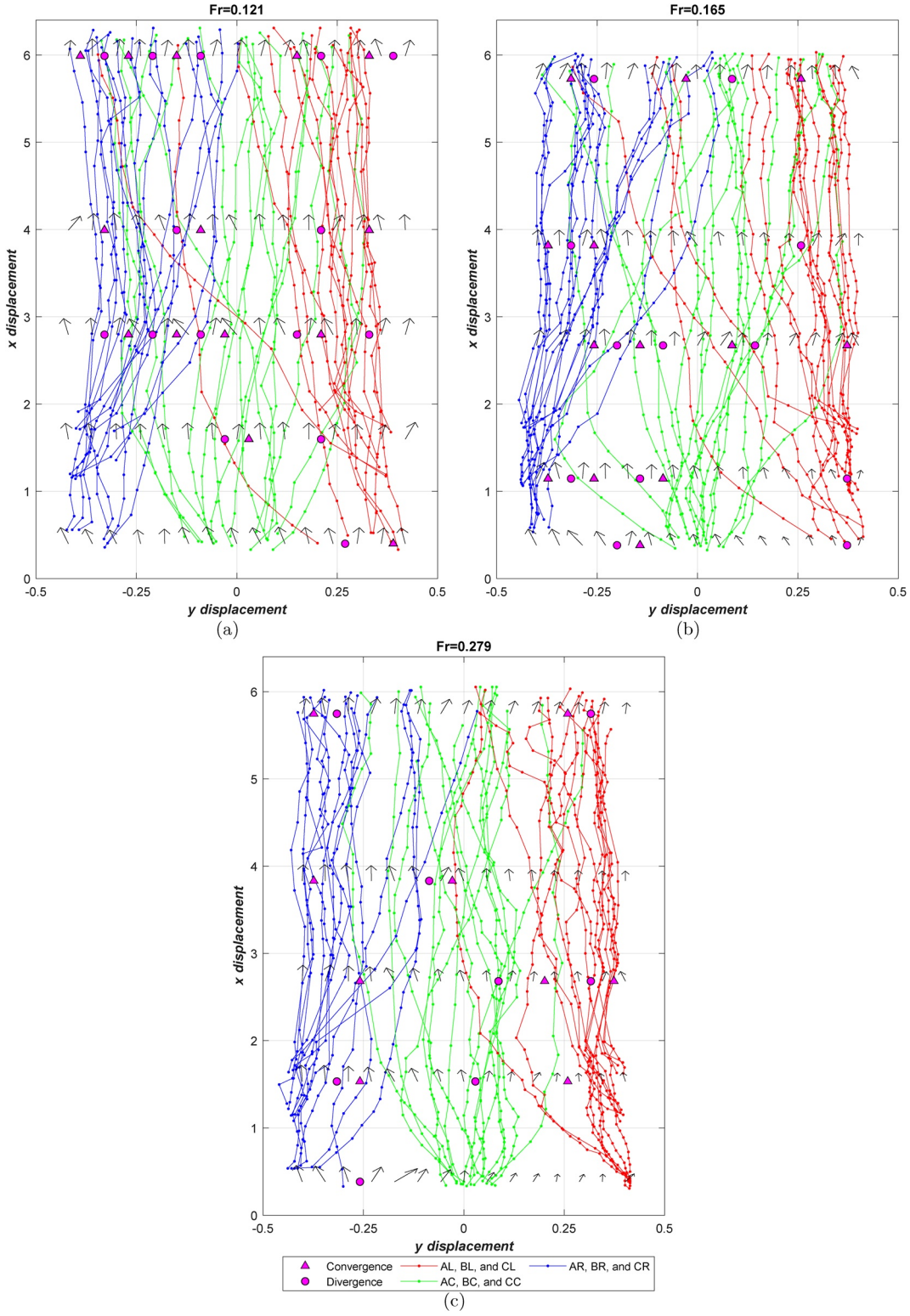

Figure 4. Planar view, for all Fr values, of LW displacement at the water surface. Blue, green, and red points and lines represent sub-groups L, C, and R, respectively. Flow velocity in the x and y direction measured at different cross-sections are represented by vectors, and magenta triangles and circles represent convergence and divergence points respectively.

immediate correlation to the y-component of velocity. Identical situation occurs for all other cross-sections where velocity was measured. Similar observations consistently with $Fr = 0.121$ can be made for $Fr = 0.165$ and $Fr = 0.279$, indicating that LW motion on the y direction is not directly caused by the y component of flow velocity.

Figure 4 also include convergence and divergence points as defined in Section 3.1. In some situations, a more concentrated amount of LW elements was observed around convergence points; for example, for $Fr = 0.121$ at $x = 3.994$, five elements each were observed in the immediate vicinity of two convergence points at y = -0.330 and 0.330, whilst at a third convergence point y = -0.090, no elements were observed. Similarly, for $Fr = 0.279$ convergence points where concentration of LW elements was high was rarely observed; for example, two convergence points at $x = 2.682$ and -0.259 showed five LW elements each, whereas a third point at $x = 0.201$ had no elements nearby. On the other hand, divergence points may show considerable amount of LW elements in the nearby areas and only in a very small number of cases (e.g., the divergence points measured for $Fr = 0.279$ at $x = 3.831$ and $x = 2.682$) no LW elements were observed. Overall, the average number of LW pieces in the proximity (i.e., in between two flow velocity measurements) of a convergence point for all cases was 3.09 (standard deviation, SD, 1.84), while it resulted 3.29 (SD 1.48), 2.92 (SD 2.10), and 3.00 (SD 1.94) when broken down for $Fr = 0.121$, $Fr = 0.165$, $Fr = 0.279$ respectively. The average number of LW elements nearing a divergence point for all tests was 3.49 (standard deviation, SD, 1.96), with the average for macro-groups A, B, and C being 3.67 (SD 1.85), 3.25 (SD 2.20), and 3.50 (SD 1.73), respectively. In summary, it was observed that neither convergence nor divergence points were preferential patterns in LW motion (e.g., high concentration of LW near convergence points and low for divergence points).

4. Analysis and Discussion

4.1. Large Wood Transport and Probability of Observation

The experimental observations of LW element trajectories and rotational/translational motions described in the previous section allow for interesting insights into the understanding of LW transportation phenomena at the water surface. First, the trajectories observed in Figure 4 are mostly concentrated in the area of the channel where the LW element was introduced and becomes even more evident for the highest Fr number. This is in agreement with field observations (Diehl, 1997) whereby LW is observed in preferential patterns along the surface of a river. This preferential LW transport may also explain, for example, why accumulations of LW at bridge piers were repeatedly observed at the same location over the years (Panici et al., 2020), although local flow conditions could have a major influence on the LW trajectories; therefore, a detailed analysis of the relationship between flow field and LW is required to fully explain this tendency. Identifying the mechanism and location of introducing a LW element into a river (e.g., from bank erosion or from uplift of elements on the floodplains) might give a broad estimation of the channel area where an element can be expected in the downstream reaches. This could provide important insights for analyses and assessments that depend on LW position or motion (e.g., likelihood of impact to riverine structures). However, it is important to note that at full-scale, results can be considered accurate when conditions similar to those tested in this paper (e.g., relatively straight channel, negligible influence from other factors such as sediment transport, boulders, vegetation) are observed in the field.

In order to provide a better understanding of the preferential patterns followed by LW, Figure 5 displays the probability density of observing a LW at any y coordinate across several cross-sections at x = 1.5, 2.5, 3.5, 4.5, and 5.5 for the three Fr conditions tested. The goodness of fit of the probability density function (pdf) in these cross-sections has been estimated through maximum likelihood estimation (MLE) of the log-likelihood function by measuring the concentration of LW element per intervals of $\Delta y = 0.05$. The figure shows that probability of observing LW at a given point in a cross-section for lower Fr values tends to display higher dispersion, whilst for the highest Fr (0.279) tested in this work, probability density is notably higher in narrower areas of the channel. It was also observed (Figure 4) that for the highest Fr the trajectories of LW elements were more streamlined than lower Fr conditions, and most elements remained within ±0.2 channel widths of their original location onto the water surface. On the other hand, for the lowest $Fr = 0.121$ this range was at a broader value, that is, approximately ±0.4 channel widths. Also, it can be observed that, for all Fr conditions, dispersion is smaller for LW elements released at the channel banks. Furthermore,

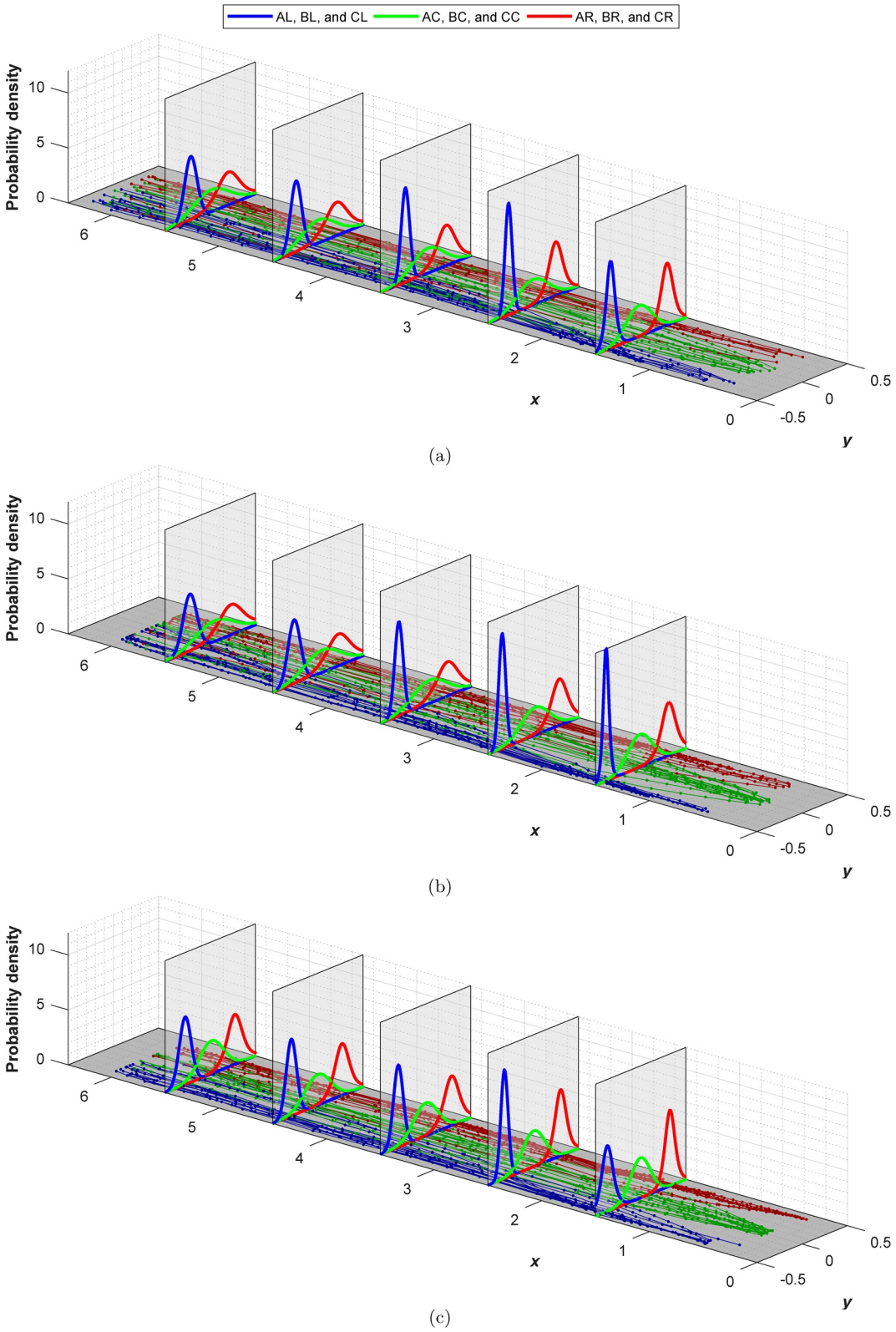

Figure 5. Estimation of probability density of observing a LW for any y coordinate for $Fr = 0.121$ (5a), $Fr = 0.165$ (5b), and $Fr = 0.279$ (5c) in five cross-sections along the x direction. LW trajectories of all tests are included in the x-y plane.

there is a slight tendency to increase the variability of probability of LW location with increasing x (i.e., pdf curves tend to get shallower and wider), although this occurs at a reduced rate for increasing Fr. The marked difference of behaviors between experimental groups observed in this study may be explained by the larger contribution of the velocity inertial forces along the x-direction: Increase in Fr will increase inertia by a quadratic power and therefore will reduce the effect of other forces along the direction perpendicular to the flow. These observations seem to be in strong agreement with De Cicco et al. (2020), who observed a narrower area occupied by LW with increasing Fr. Although the range of Fr studied by De Cicco et al. (2020) is different from this study, that is, occurred for higher Fr values, it would seem to provide the same tendency observed in this study. Moreover, it is interesting to observe that in De Cicco et al. (2020), in the condition for $Fr = 0.30$ the portion of channel where LW could be observed was, approximately, $-0.25< y <0.25$. This is a striking parallel with experimental group CC - that is, $Fr = 0.279$ and elements released at the flume centerline, where the majority of elements was observed broadly in the same interval, and where there is on average a 97% of probability of observing a LW released at the centerline, according to the probability distribution shown in Figure 5. This would confirm that Fr can affect distribution of elements and that the possible range of observed elements will lie in a well-defined part of the channel. Finally, an important observation regards the transient motion when LW elements are released onto the water surface. Whilst a fully developed transport of LW can be found in a relatively narrow channel area depending on the release point (as mentioned above), its accurate location and, thus, potential ability to predict and model downstream transport, depend strongly on the initial displacement along the transient motion of length 1 channel width on the x-direction. This well-marked observation might be explained by the little or no inertia of LW elements when released onto the water surface: Any small change in the applied forces would incur in a change of motion that can be significant. Although this transient motion seems to be intrinsically stochastic, its understanding would pave the way to accurate predictions of downstream trajectories.

The different mechanism by which LW elements are conveyed on the water surface (as shown in Figure 3) highlights that these motions are dependent on the hydrodynamic actions, although there is no immediate correlation between secondary cells and LW trajectories. According to the theory by Diehl (1997) and Bradley et al. (2005), convergence points were postulated to systematically gather LW elements in this narrow parts of the channel, since secondary currents were considered to play a primary role in the motion of LW elements. Nevertheless, the experimental observations in this work showed that this theory might be inaccurate in similar full-scale conditions, for example, straight, nearly uniform channels. Only a few convergence points in the three Fr conditions tested in the flume showed some gathering of elements. On the other hand, many other convergence points saw little or no LW elements being conveyed through them, whilst divergence points - that, by extension of the theory by Diehl (1997) leave only a single point of equilibrium that is, intrinsically unstable, were in some occasions observed with a large number of transiting elements. It is also worth highlighting that convergence points showed a considerable variability, resulting in a coefficient of variation (CV) of 59.7%, whilst the average number of LW observed in their proximity, 3.09 LW per point, was no higher than any other section in the channel. Interestingly, the average number of LW elements traveling near a divergence point (3.49) was higher than convergence points, in contrast with the hypothesis that the flow secondary cells are the main drivers of LW location on the river surface. In addition, there was no significant difference between LW elements observed near convergence and divergence points, whereby p-value resulted in $p = 0.3818$ indicating that the null hypothesis (i.e., that there was no significant difference between convergence and divergence points) is true. Therefore, this shows that the theory by Diehl (1997) and Bradley et al. (2005) in straight channels is incomplete and needs to be integrated in a better-defined mechanistic model. On the other hand, this paper could not establish the accuracy of the convergence points theory in river bends, since tests were not carried out for curved channels.

4.2. Theoretical Model

The observations of the experimental tests in this paper have been used to develop a theoretical model in order to explain and predict the LW elements trajectories beyond qualitative analysis and based on physics. Consider a LW element on the water surface of a straight channel, simplified by a cylindrical shape of length L, diameter d and density ρ_W. The element is also tilted with respect to the y-direction by an angle θ and is traveling at a velocity $\mathbf{v_{L0}}$, of components in both x and y directions. Figure 6 shows a sketch of a LW element, its geometry, and the flow velocity. The main assumption in this analysis is that the change

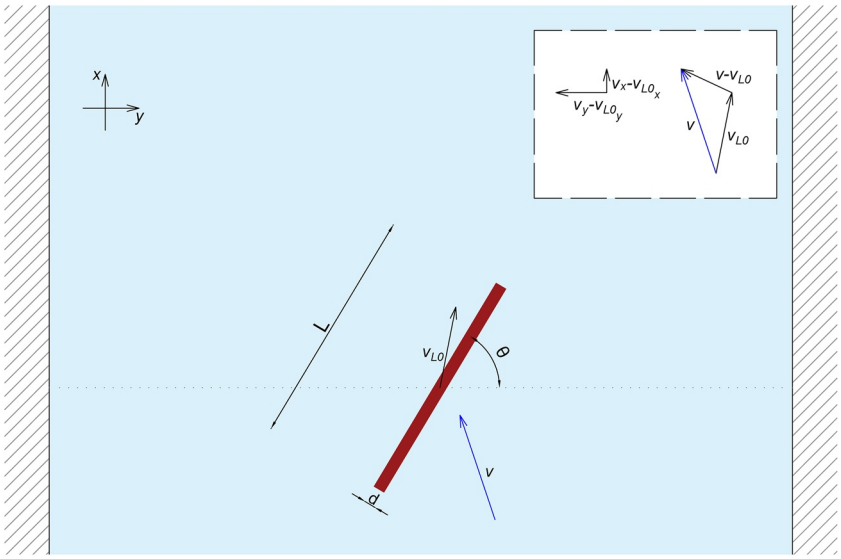

Figure 6. Sketch of an idealized cylindrical LW of length L and diameter d, tilted to the horizontal with an angle θ, traveling at a velocity $\mathbf{v_{L0}}$, for a flow velocity v. The sketch also shows the net components of velocity (i.e., $\mathbf{v_y} - \mathbf{v_{L0_y}}$ and $\mathbf{v_x} - \mathbf{v_{L0_x}}$) to be used for Equation 8.

in trajectory of waterborne LW is mainly caused by a change in local hydrodynamic actions to the floating elements. Whenever the relative velocity between flow ($\mathbf{v}$) and LW ($\mathbf{v_{L0}}$) is non-zero in magnitude and direction, that is, $\mathbf{v}$-$\mathbf{v_{L0}} \neq 0$, the flow will exert a net drag force $\mathbf{F_D}$ on the LW element. For the purpose of this study, drag is assumed to be the main force acting on the floating element so that other forces (except for virtual mass) can be neglected, and therefore the LW will have an accelerated motion:

$$\mathbf{F_D} = m_L \mathbf{a_L} \tag{4}$$

where m_L is the LW mass and $\mathbf{a_L}$ its acceleration, that can simply be defined as $\frac{d\mathbf{v_L}}{dt}$. Considering the assumption of a cylindrical piece, the mass m_L is given as the product between a cylinder volume and the LW density. In addition, virtual mass is added to (4), as it is an additional component to the resisting forces (Panici & de Almeida, 2020a), and the density of the floating solid is rewritten as $\rho_{eq} = \rho_L(1 + C_M)$, where C_M is the coefficient of added mass; it should be noted that this equivalent density is only valid for floating LW (i.e., $\rho_L < \rho$). Using the canonical formula for drag force and the above defined mass, Equation 4 becomes:

$$\rho_L \frac{d^2\pi}{4} L\left(1 + C_M\right)\frac{d\mathbf{v_L}}{dt} = \frac{1}{2}\rho C_D A_L \left(\mathbf{v} - \mathbf{v_{L0}}\right)\left|\mathbf{v} - \mathbf{v_{L0}}\right|, \tag{5}$$

where ρ is the density of water, $\mathbf{v}$ is the water velocity, $\mathbf{v_{L0}}$ the LW velocity at the initial condition, C_D the coefficient of drag of the LW and A_L the area of the LW perpendicular to the vector $\mathbf{v} - \mathbf{v_{L0}}$. Equation 5 can be made explicit for the acceleration:

$$\frac{d\mathbf{v_L}}{dt} = \frac{2C_D\rho A_L\left(\mathbf{v} - \mathbf{v_{L0}}\right)\left|\mathbf{v} - \mathbf{v_{L0}}\right|}{\rho_L d^2 \pi L\left(1 + C_M\right)}. \tag{6}$$

At this point, Equation 6 can be split into the x and y components. Since the cylinder is modeled as a floating object, the area perpendicular to the flow will be the submerged component and is given by:

$$A_{L_x} = \frac{\rho_L}{\rho}\left(Ld\sin\theta + \frac{d^2\pi}{4}\cos\theta\right),$$
$$A_{L_y} = \frac{\rho_L}{\rho}\left(Ld\cos\theta + \frac{d^2\pi}{4}\sin\theta\right), \quad (7)$$

where the ratio ρ_L / ρ provides the submergence of the LW and under the condition that $\rho_L \leq \rho$ (i.e., the LW is floating). In Equation 7 it should be noticed that (ignoring trigonometric functions for either area) $\frac{\rho_L}{\rho}\frac{d^2\pi}{4}$ is the exact relationship for the submerged circular face of the cylinder; nevertheless, an analytical solution for the longitudinal submerged area is not available. In this case it is possible to approximate the submerged longitudinal area of the cylinder to $\frac{\rho_L}{\rho}dL$. Such approximation would lead to a maximum error of ±6% for $\frac{\rho_L}{\rho} \approx 0.2$ and 0.8, whereas for $\frac{\rho_L}{\rho} = 0.5$, which is close to the density ratio used for this study, the error is null. Therefore, it is a reasonable assumption to employ Equation 7 to compute the submerged area perpendicular to the water flow, which ensures the use of an analytical function of the longitudinal area and has limited loss of accuracy (up to 6%). Equation 7 can be substituted in Equation 6, leading to:

$$\frac{d\mathbf{v}_{\mathbf{L_x}}}{dt} = \frac{2C_D\left(L\sin\theta + \frac{d\pi}{4}\cos\theta\right)\left(\mathbf{v_x} - \mathbf{v_{L0_x}}\right)\left|\mathbf{v_x} - \mathbf{v_{L0_x}}\right|}{d\pi L\left(1 + C_M\right)},$$
$$\frac{d\mathbf{v}_{\mathbf{L_y}}}{dt} = \frac{2C_D\left(L\cos\theta + \frac{d\pi}{4}\sin\theta\right)\left(\mathbf{v_y} - \mathbf{v_{L0_y}}\right)\left|\mathbf{v_y} - \mathbf{v_{L0_y}}\right|}{d\pi L\left(1 + C_M\right)}, \quad (8)$$

where $\mathbf{v_{L0_x}}$, $\mathbf{v_{L0_y}}$, $\mathbf{v_x}$ and $\mathbf{v_y}$ are, respectively, the x and y component of the LW velocity and flow velocity, as shown in Figure 6. Equation 8 effectively provides the equation for the acceleration of a LW element of cylindrical size. This equation assumes that the velocity distribution along the surface of the LW is uniform. In reality, it is unlikely to observe this uniformity, which can also be considered the cause for rotation and tilting of LW elements as observed in Figure 3, but for the purpose of this theoretical analysis, the velocity uniformity assumption was made. For short distances, it can be assumed that the acceleration will remain constant. As a result, the displacement $\mathbf{x_L}$ and $\mathbf{y_L}$ of a LW piece (calculated at its center of mass) in a sufficiently short time interval t from the original position x_0 and y_0 (i.e., the location where the net drag force will accelerate the cylindrical LW), is found as:

$$\mathbf{x_L} = x_0 + \mathbf{v_{L0_x}}t + \frac{1}{2}\left(\frac{d\mathbf{v}_{\mathbf{L_x}}}{dt}\right)t^2,$$
$$\mathbf{y_L} = y_0 + \mathbf{v_{L0_y}}t + \frac{1}{2}\left(\frac{d\mathbf{v}_{\mathbf{L_y}}}{dt}\right)t^2. \quad (9)$$

Equations 8 and 9 have been applied to a random sample of 30 elements across all experimental groups in which flow velocity measurements and LW tracking was available, some of which were already shown in Figure 3. LW motion prediction could only be conducted at these sections since Equation 8 depends on the measured values of flow velocity and Equation 9 is only defined for small changes in space and time. Water velocity $\mathbf{v_x}$ and $\mathbf{v_y}$ measurement were provided by the ADV and averaged when two or more punctual measurements were crossed by a LW element, the angle θ was estimated by the coordinates of the two ends of each LW piece, the initial velocity of the LW $\mathbf{v_{L0_x}}$ and $\mathbf{v_{L0_y}}$ was also estimated from the analysis of video recordings and the elapsed time was known from the video footage sampling frequency. For the purpose of the calculations, the coordinates x_0 and y_0 were computed at the center of mass of a LW element in the video frame captured before crossing the flume section where the superficial velocity was known. The two coefficients of drag and added mass have been kept constant and computed as $C_D = 1$, typical of cylindrical elements in water (Gippel et al., 1996), and $C_M = 0.5$.

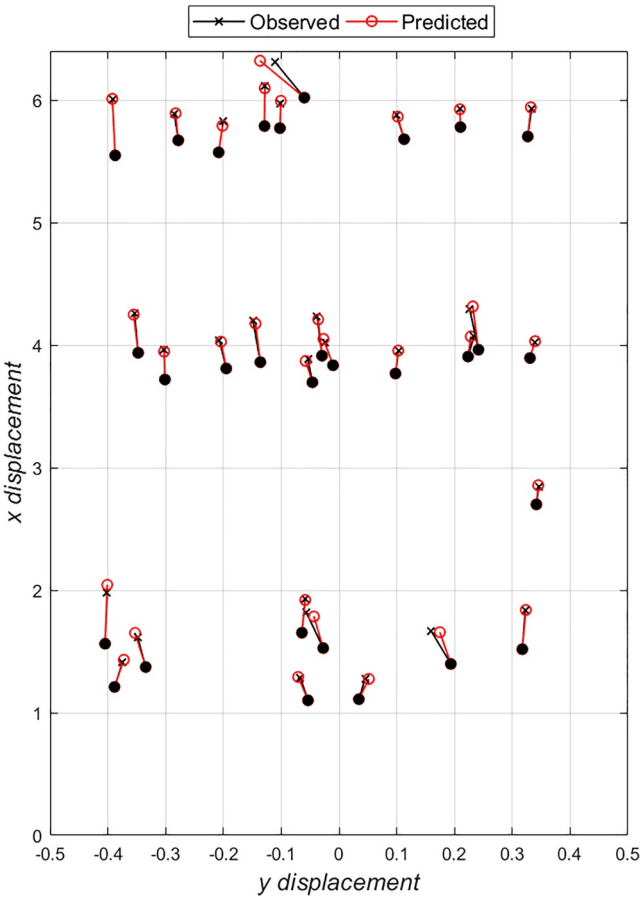

Figure 7. Comparison between observed trajectories (black line and crosses) and predicted trajectories (red line and circles) for random tests from all experimental groups. Each line originates at points of coordinates (x_0, y_0), solid black circle, that is, used for calculations of Equation 9.

Table 2
Error of Model Predictions for all Experimental Groups

Fr		Average error	Standard deviation	CV	Standard error
0.121	x	5.85%	4.49%	76.68%	1.50%
	y	23.51%	19.75%	83.99%	6.58%
	$x-y$	6.44%	4.26%	66.22%	1.42%
0.165	x	7.01%	4.62%	65.83%	1.39%
	y	23.28%	12.48%	53.63%	3.76%
	$x-y$	7.32%	4.36%	59.54%	1.31%
0.279	x	6.61%	4.01%	60.61%	1.27%
	y	30.58%	13.32%	43.54%	4.21%
	$x-y$	7.33%	4.09%	55.77%	1.29%
All	x	6.53%	4.41%	67.50%	0.80%
	y	25.78%	15.65%	60.68%	2.86%
	$x-y$	7.06%	4.26%	60.36%	0.78%

The model prediction was, in most situations, very close to the observed values. Figure 7 shows the predicted motion of the center of mass of LW elements calculated according to Equation 9, and the observed LW, for sections immediately upstream and downstream of flow velocity measurements in the flume. Each line represents a LW element before and after said cross-sections for both observed and modeled trajectories. The prediction of LW trajectories in Figure 7 confirms that the model in Equations 8 and 9 reasonably predicts the displacement of LW elements with limited loss of accuracy. Defining the measurement error as the ratio between the distance of the observed and predicted centers of mass (i.e., $x_{L(\mathrm{obs})}$-$x_{L(\mathrm{pred})}$ and $y_{L(\mathrm{obs})}$-$y_{L(\mathrm{pred})}$) and the observed distance traveled (i.e., $x_{L(\mathrm{obs})}$-x_0 and $y_{L(\mathrm{obs})}$-y_0), Table 2 provides a detailed overview of the prediction error of the model for all predicted elements. On average, the overall error was 7.06% (standard deviation 4.26%, standard error 0.78%), which indicates that the prediction error was relatively small and tends to be relatively consistent, considering the values of coefficient of variation (CV) and standard error that have been computed. The error on the x direction is typically small (6.53% on average), whilst the error on the y direction is relatively larger (on average 25.78%), although this is likely due to the higher varying degree of water velocity on the y direction and the much smaller magnitude compared to $\mathbf{v_x}$, which may result in comparatively much larger velocity gradients. Furthermore, the highest errors were observed for elements that had the largest distances or time-steps between calculation. This is expected, as the model is meant to work for small time-steps in the assumption that the acceleration caused by the hydrodynamic forces is constant only for a small distance. Thus, this may have a negative effect on the assumptions made for the model construction that has led to a higher degree of error for the y displacement. The results displayed in Figure 7 and Table 2 showed that the model is reliable for similar flow and LW conditions, and that it produces realistic results even when including a considerable wide range of velocities, such that was measured at the surface. The accuracy of the model seems not affected by the different Fr levels, whereby the average error (and its standard deviation) for each x, y and $x-y$ component is consistent throughout the three Fr values observed. This would suggest that Equations 8 and 9 work well at the different levels of Fr tested in this work, that is, $0.121 \leq Fr \leq 0.279$. The relative accuracy of the model prediction also indicates that full-scale applications could benefit of the use of hydrodynamic models (which are easier and cheaper than measuring in the field) for estimating areas in the channel where LW transport is likely and further research on this topic is encouraged.

However, caution should be used when the above conditions are not met (e.g., velocity varies rapidly in a cross-section and between nearing sections), as they may produce inaccurate results. On the other hand, when flow conditions are gradually varied and velocity is known at short distances, it would be possible to predict the trajectory change of LW elements. Therefore, this works provide a first simplified approach for the estimation of LW trajectories. Nevertheless, this model is only the first attempt to describe the motion of LW. Further studies and experiments are needed in order to fully develop the above model. An important component to be included and that has been neglected in this study is the tilting and rotation of the LW elements. This will provide a full model of motion (including rotation together with translation) as well as enhancing Equation 8 with the change in θ due to the rotation of the

element. In this study, the change of θ has not been included, but it will be necessary for a comprehensive system of equations. Other important considerations will need to include the hydrodynamics effects of varying velocity along the LW element, which will change the effect of the exerted drag force. The drag coefficient used for this study has been assumed constant due to Reynolds invariance and based on previous studies; however, since C_D might change with Reynolds number, further studies should be conducted to provided a more refined estimation. Moreover, other considerable factors for the correct prediction of LW motion - such as interaction with river banks, river planimetry, and LW characteristics, should be included and tested in future research. Developing a set of equations inclusive of all factors affecting LW motion will enable prediction for full-scale analysis by using the output of hydrodynamic models.

4.3. Applications and Future Outlook

The work shown in this paper has described some of the key-phenomena associated with LW transport and provided a first approach for prediction of LW motion. However, further research is necessary to provide a full picture of the phenomena of LW transport in rivers and its practical applications, especially on some of the simplifications that have been employed. For example, tests should be carried out on curved reaches to evaluate the effect of flow on LW in bends; LW with different shapes (e.g., branches, root wads) should be tested for comparison; inclusion of natural elements (e.g., boulders, sediment transport) and infrastructures (e.g., bridges); input of LW with different angles or initial conditions. Froude similarity and scaling through dimensionless quantities as discussed in the dimensional analysis provided similitude between model and prototype. The assumed Reynolds invariance was also a reasonable mitigation to scaling issues related to viscous forces; however, further investigation should be considered for potential changes in drag force at different Reynolds numbers.

Potential applications of the results from this work and future research may apply to studies in which LW transport is a crucial component, for example, by predicting preferential patterns in a river reach. These applications include river restoration projects, in which LW reintroduction is used for biodiversity; therefore, correct understanding of LW transport patterns will aid planning and designing the LW input for this type of projects. Other applications include LW protection measures at bridges or other structures, since these rely on trapping or diverting LW, such as racks or fins and sweepers (e.g., Panici & Kripakaran, 2021; Schalko et al., 2019b). Also, risk assessment to LW impact forces and scour actions at structures may depend on likelihood of impact or trapping (Schalko et al., 2019a) and this study will therefore provide a more accurate assessment, since it will enable estimation of areas of the channel prone to LW transport and expected LW velocities. Accurate prediction and understanding of transport of LW recruited by a river are dependent on the transient motion at the initial stages of the element release on the water surface; thus, further investigation is required for a better understanding of these phenomena.

5. Conclusions

Understanding and predicting the motion of LW on the river surface is of primary importance for estimating the impact of LW in rivers for flood defense and habitat restoration, to assess and design mitigation measures for existing structures (e.g., bridges or dams), to enhance design of future structures. This article provides a detailed overview of the main phenomena observed during flume experimental campaigns for the motion of LW at the water surface and its interactions with superficial water velocity. Consistently with field observations, LW was observed to travel along preferential positions in a river reach, depending on the point where the LW element was released. This tendency is further noticeable with the increase of the flow Froude number Fr, whereby higher Fr result in elements transported in well defined narrow areas of the channel (except for a few elements). More importantly, it was observed that most elements after an initial transient motion of approximately 1 channel width, kept the trajectory at which they are traveling with limited changes in the direction perpendicular to the flow, although over a long distance it can be expected that location of LW pieces on the y-direction will be fully mixed. This observation implies two important considerations: First, that the initial location of the LW release will have crucial importance for the expected location at fully developed conditions; second, for prediction purposes when an element observed on the water surface is no longer on a transient motion, the approximate estimation of its future location can be limited to a narrow section of the channel.

Several mechanism of motion at the water surface were identified. The most frequent observations included LW elements being tilted or completely rotated and placed perpendicularly to the flow direction. However, in most occasions LW reverted to a tilted or straight position, suggesting that a normal orientation to the flow might be relatively unstable. In less frequent observations, LW elements retained a straight orientation (i.e., parallel) relatively to the flow or completely rotated (i.e., perpendicular to the flow).

The experimental work shown in this study for the first time shed a light on relationship between the trajectories of LW and flow velocity convergence points at the water surface. The tests showed that this theory is inconclusive, since only a limited amount of LW was observed crossing these points, whereas it was postulated that the large majority of LW elements should have been observed here. Furthermore, expanding on this theory, the divergence points (i.e., where velocity of secondary cells diverges) would supposedly provide an unstable condition for retaining LW, but experimental observations revealed that many element could be observed, with minimal differences to convergence points.

A new simplified model has been proposed in this paper, whereby the motion of LW can be described by local accelerations induced by change in the LW-flow relative velocity, which, in turn, induces a drag force applied to the LW element. Experimental results showed that the model can predict the displacement of a LW depending on its original position and observed velocity, while errors are negligible. The limited loss of accuracy of the model suggests that its application is a viable option to describe the motion of LW at the water surface.

The results shown in this work will provide qualitative and quantitative tools for the estimation and prediction of LW transport at the river surface. The paper will also pave the way for further experiments and theoretical developments to include those aspects that have not investigated in this work (for example, curved reaches, vegetation, boulders) and that will be beneficial for a thorough understanding of LW transport in rivers.

Data Availability Statement

Data supporting the results presented in this paper are openly available from the University of Exeter repository at doi: https://doi.org/10.24378/exe.3383.

Acknowledgments
The author is grateful for the financial support of the UK Natural Environment Research Council (NERC), grant NE/V003402/1, and of the UK Engineering and Physical Sciences Research Council (EPSRC), through the Center for Doctoral Training in Sustainable Infrastructure Systems (CDT-SIS), grant EP/L01582X/1. The author is also thankful to Dr Toru Tsuzaki and Mr Karl Scammell of the University of Southampton Hydraulic Laboratory for the material help in carrying out the experiments, and to the students Fiona and Pierre for the practical help with the experiments. Finally, the author is immensely grateful to his PhD supervisor at the University of Southampton, Dr Gustavo de Almeida, for the guidance during his doctoral studies when the experiments in this paper were carried out. The author is also thankful to the three anonymous reviewers whose comments substantially improved the quality of this manuscript.

References

Abbe, T. B., & Montgomery, D. (1996). Large woody debris jams, channel hydraulics and habitat formation in large rivers. *Regulated Rivers*, *12*, 201–221. https://doi.org/10.1002/(sici)1099-1646(199603)12:2/3<201::aid-rrr390>3.0.co;2-a

Bocchiola, D., Rulli, M., & Rosso, R. (2008). A flume experiment on the formation of wood jams in rivers, *Water Resources Research*, *44*, W02408. https://doi.org/10.1029/2006WR005846

Bradley, J. B., Richards, D. L., & Bahner, C. D. (2005). *Debris control structures - evaluation and countermeasures*. DC, Federal Highway Administration, U.S. Department of Transportation.

Braudrick, C. A., Grant, G. E., Ishikawa, Y., & Ikeda, H. (1997). Dynamics of wood transport in streams: A flume experiment. *Earth Surface Processes and Landforms*, *22*, 669–683. https://doi.org/10.1002/(sici)1096-9837(199707)22:7<669::aid-esp740>3.0.co;2-l

Comiti, F., Luciá, A., & Rickenmann, D. (2016). Large wood recruitment and transport during large floods: A review. *Geomorphology*, *269*, 23–39. https://doi.org/10.1016/j.geomorph.2016.06.016

Crosato, A., Rajbhandari, N., Comiti, F., Cherradi, X., & Uijttewaal, W. (2013). Flume experiments on entrainment of large wood in lowland rivers. *Journal of Hydraulic Research*, *51*, 581–588. https://doi.org/10.1080/00221686.2013.796573

Curran, J. (2010). Mobility of large woody debris (LW) jams in a low gradient channel. *Geomorphology*, *116*, 320–329. https://doi.org/10.1016/j.geomorph.2009.11.027

De Cicco, P. N., Paris, E., Solari, L., & Ruiz-Villanueva, V. (2020). Bridge pier shape influence on wood accumulation: Outcomes from flume experiments and numerical modeling. *Journal of Flood Risk Management*, *13*. https://doi.org/10.1111/jfr3.12599

Diehl, T. H. (1997). *Potential drift accumulation at bridges, federal highway administration*. DC, U.S. Department of Transportation.

Ebrahimi, M., Djordjević, S., Panici, D., Tabor, G., & Kripakaran, P. (2020). A method for evaluating local scour depth at bridge piers due to debris accumulation. *Proceedings of the Institution of Civil Engineers - Bridge Engineering*, *173*, 86–99. https://doi.org/10.1680/jbren.19.00045

Ebrahimi, M., Kripakaran, P., Prodanovic, D., Kahraman, R., Riella, M., Tabor, G., et al. (2018). Experimental study on scour at a sharp-nose bridge pier with debris blockage. *Journal of Hydraulic Engineering*, *144*. https://doi.org/10.1061/(asce)hy.1943-7900.0001516

Furlan, P., Pfister, M., Matos, J., Amado, C., & Schleiss, A. J. (2018). Experimental repetitions and blockage of large stems at ogee crested spillways with piers. *Journal of Hydraulic Research*, *57*, 250–262. https://doi.org/10.1080/00221686.2018.1478897

Gippel, C., Finlayson, B., & O'Neill, I. (1996). Distribution and hydraulic significance of large woody debris in a lowland Australian river. *Hydrobiologia*, *318*, 179–194. https://doi.org/10.1007/bf00016679

Gregory, K., Davis, R., & Tooth, S. (1993). Spatial distribution of coarse woody debris dams in the Lymington Basin. *Geomorphology*. *6*, 207–224. https://doi.org/10.1016/0169-555x(93)90047-6

Gschnitzer, T., Gems, B., Mazzorana, B., & Aufleger, M. (2017). Toward a robust assessment of bridge clogging processes in flood risk management. *Geomorphology*, *279*, 128–140. https://doi.org/10.1016/j.geomorph.2016.11.002

Gurnell, A. M., England, J., & Burgessgamble, L. (2019). Trees and wood: Working with natural river processes. *Water and Environment Journal*, *33*, 342–352. https://doi.org/10.1111/wej.12426

Hassan, M. A., Bird, S., Reid, D., & Hogan, D. (2016). Simulated wood budgets in two mountain streams. *Geomorphology*, *259*, 119–133.

Heller, V. (2011). Scale effects in physical hydraulic engineering models. *Journal of Hydraulic Research*, *49*, 293–306. https://doi.org/10.1080/00221686.2011.578914

Lagasse, P., Colopper, P., Zevenbergen, L., Spitz, W., & Girard, L. (2010). *Effects of debris on bridge pier scour*. DC, National Cooperative Highway Research Program, Transportation Research Board.

Lassettre, N. S., & Kondolf, G. M. (2012). Large woody debris in urban stream channels: Redefining the problem. *River Research and Applications*, *28*, 1477–1487. https://doi.org/10.1002/rra.1538

Lyn, D., Cooper, T., Condon, C., & Gan, G. (2007). *Factors in debris accumulation at bridge piers*. DC, Federal Highway Administration, U.S. Department of Transportation.

Lyn, D., Cooper, T., Yi, Y., Sinha, R., & Rao, A. (2003). *Debris accumulation at bridge crossing: Laboratory and field studies*. DC, Federal Highway Administration, U.S. Department of Transportation.

Mao, L., Ravazzolo, D., & Bertoldi, W. (2020). The role of vegetation and large wood on the topographic characteristics of braided river systems. *Geomorphology*, *367*, 107299. https://doi.org/10.1016/j.geomorph.2020.107299

Mazzorana, B., Hübl, J., Zischg, A., & Largiader, A. (2011). Modeling woody material transport and deposition in alpine rivers. *Natural Hazards*, *56*, 425–449. https://doi.org/10.1007/s11069-009-9492-y

Pagliara, S., & Carnacina, I. (2011). Influence of wood debris accumulation on bridge pier scour. *Journal of Hydraulic Engineering*, *137*, 254–261. https://doi.org/10.1061/(asce)hy.1943-7900.0000289

Pagliara, S., & Carnacina, I. (2013). Bridge pier flow field in the presence of debris accumulation. *Proceedings of the Institution of Civil Engineers - Water Management*, *166*, 187–198. https://doi.org/10.1680/wama.11.00060

Panici, D., & de Almeida, G. A. M. (2018). Formation, growth, and failure of debris jams at bridge piers. *Water Resources Research*, *54*, 6226–6241. https://doi.org/10.1029/2017WR022177

Panici, D., & de Almeida, G. A. M. (2020a). A theoretical analysis of the fluid–solid interactions governing the removal of woody debris jams from cylindrical bridge piers. *Journal of Fluid Mechanics*, *886*. https://doi.org/10.1017/jfm.2019.1048

Panici, D., & de Almeida, G. A. M. (2020b). The influence of pier geometry and debris characteristics on the accumulation of woody debris at bridge piers. *Journal of Hydraulic Engineering*, *146*, 04020041. https://doi.org/10.1061/(ASCE)HY.1943-7900.0001757

Panici, D., & Kripakaran, P. (2021). Trapping large wood debris in rivers: Experimental study of novel debris retention system. *Journal of Hydraulic Engineering*, *147*, 04020101. https://doi.org/10.1061/(ASCE)HY.1943-7900.0001859

Panici, D., Kripakaran, P., Djordjević, S., & Dentith, K. (2020). A practical method to assess risks from large wood debris accumulations at bridge piers. *The Science of the Total Environment*, *728*, 728. https://doi.org/10.1016/j.scitotenv.2020.138575

Pfister, M., Capobianco, D., Tullis, B., & Schleiss, A. J. (2013). Debris-blocking sensitivity of piano key weirs under reservoir-type approach flow. *Journal of Hydraulic Engineering*, *139*, 1134–1141. https://doi.org/10.1061/(asce)hy.1943-7900.0000780

Ruiz-Villanueva, V., Mazzorana, B., Bladé, E., Bürkli, L., Iribarren-Anacona, P., Mao, L., et al. (2019). Characterization of wood-laden flows in rivers. *Earth Surface Processes and Landforms*, *44*, 1694–1709. https://doi.org/10.1002/esp.4603

Ruiz-Villanueva, V., Piégay, H., Gaertner, V., Perret, F., & Stoffel, M. (2016). Wood density and moisture sorption and its influence on large wood mobility in rivers. *Catena*, *140*, 182–194. https://doi.org/10.1016/j.catena.2016.02.001

Ruiz-Villanueva, V., Piégay, H., Gurnell, A. M., Marston, A., & Stoffel, M. (2016). Recent advances quantifying the large wood dynamics in river basins: New methods and remaining challenges. *Review of Geophysics*, *54*, 611–652. https://doi.org/10.1002/2015rg000514

Schalko, I., Schmocker, L., Weitbrecht, V., & Boes, R. M. (2018). Backwater rise due to large wood accumulations. *Journal of Hydraulic Engineering*, *144*. https://doi.org/10.1061/(asce)hy.1943-7900.0001501

Schalko, I., Schmocker, L., Weitbrecht, V., & Boes, R. M. (2019a). Laboratory study on wood accumulation probability at bridge piers. *Journal of Hydraulic Research*, *58*, 566–581. https://doi.org/10.1080/00221686.2019.1625820

Schalko, I., Schmocker, L., Weitbrecht, V., & Boes, R. M. (2019b). Risk reduction measures of large wood accumulations at bridges. *Environmental Fluid Mechanics*, *20*, 485–502. https://doi.org/10.1007/s10652-019-09719-4

Schmocker, L., & Hager, W. H. (2011). Probability of drift blockage at bridge decks. *Journal of Hydraulic Engineering*, *137*, 470–479. https://doi.org/10.1061/(asce)hy.1943-7900.0000319

Schmocker, L., & Weitbrecht, V. (2013). Driftwood: Risk analysis and engineering measures. *Journal of Hydraulic Engineering*, *139*, 683–695. https://doi.org/10.1061/(asce)hy.1943-7900.0000728

Sedell, J., Bisson, P., & Gregory, S. (1988). *From the forest to the sea: A story of fallen trees. What we know about large trees that fall into streams and rivers?* U.S. Department of Agriculture, Forest Service U.S. Department of the Interior, Bureau of Land Management.

Wallerstein, N., Thorne, C. R., & Abt, S. R. (1997). *Debris control at hydraulic structures in selected areas of the United States and Europe*. U.S. Army Engineer Waterways Experiment Station.

Wilcox, A., & Wohl, E. (2006). Flow resistance dynamics in step-pool stream channels: 1. large woody debris and controls on total resistance. *Water Resources Research*, *42*, W05418. https://doi.org/10.1029/2005wr004277